Anisotropic Shape Changes of Silica Nanoparticles Induced in Liquid with Scanning Transmission Electron Microscopy

Jovana Zečević, Justus Hermannsdörfer, Tobias Schuh, Krijn P. de Jong, and Niels de Jonge**

***L**iquid-phase transmission electron microscopy (TEM) is used for in-situ imaging of nanoscale processes taking place in liquid, such as the evolution of nanoparticles during synthesis or structural changes of nanomaterials in liquid environment. Here, it is shown that the focused electron beam of scanning TEM (STEM) brings about the dissolution of silica nanoparticles in water by a gradual reduction of their sizes, and that silica redeposites at the sides of the nanoparticles in the scanning direction of the electron beam, such that elongated nanoparticles are formed. Nanoparticles with an elongation in a different direction are obtained simply by changing the scan direction. Material is expelled from the center of the nanoparticles at higher electron dose, leading to the formation of doughnut-shaped objects. Nanoparticles assembled in an aggregate gradually fuse, and the electron beam exposed section of the aggregate reduces in size and is elongated. Under TEM conditions with a stationary electron beam, the nanoparticles dissolve but do not elongate. The observed phenomena are important to consider when conducting liquid-phase STEM experiments on silica-based materials and may find future application for controlled anisotropic manipulation of the size and the shape of nanoparticles in liquid.*

Dr. J. Zečević, Prof. K. P. de Jong
Inorganic Chemistry and Catalysis
Debye Institute of Nanomaterials Science
Utrecht University
3584 CG Utrecht, The Netherlands
E-mail: J.Zecevic@uu.nl

Dr. J. Hermannsdörfer,[+] Dr. T. Schuh,[++] Prof. N. de Jonge
INM–Leibniz Institute for New Materials
Campus D2 2, 66123 Saarbrücken, Germany
E-mail: niels.dejonge@leibniz-inm.de

Prof. N. de Jonge
Department of Physics
University of Saarland
Campus A5 1, 66123 Saarbrücken, Germany

[+]Present address: Nanoinitiative Bayern GmbH, 97074 Würzburg, Germany
[++]Present address: Enovos Deutschland SE, 66121 Saarbrücken, Germany

DOI: 10.1002/smll.201602466

1. Introduction

Transmission electron microscopy (TEM) has been a key technique for studying the nanometer-scale morphology of a broad range of samples, for example, catalytic nanoparticles.[1] However, conventional TEM requires the specimen to be placed in the vacuum of the electron microscope, and thus requires solid samples. With recently developed liquid-phase TEM, samples can be now imaged in a liquid environment.[2] Liquids are enclosed in specially designed liquid cells usually composed of silicon chips with thin electron transparent silicon nitride windows.[3] It is also possible to image liquid samples in an open vacuum chamber using pump-limiting apertures,[2e] or to study low vapor pressure liquids with standard TEM.[4] The closed cell type is becoming increasingly popular as it has the potential to provide unique insight into dynamic processes at the nanometer scale, such as nucleation and growth of nanoparticles,[5] dynamic movements of

nanoparticles,[3c,d,6] electrochemical deposition and growth of nanoparticles,[7] biomineralization,[5g] and can also be used to study biological function.[8] One of the key challenges liquid-phase TEM faces is to discriminate the phenomena under investigation from electron beam induced effects, such as radiolysis of water in aqueous systems, resulting in the formation of reactive species including e_{aq}^-, $H^\bullet$, $OH^\bullet$, H_2, H_2O_2, H^+, OH^-.[3f,9] The evolution of H_2 through water radiolysis has been linked to the bubble formation within the cell, the creation of e_{aq}^- may trigger the reduction of metal ions in the aqueous solutions, while OH^- and H^+ species can locally change the chemistry of the liquid under examination.[9a] Electron beam induced reduction of metal ions has been the focus of a number of studies in the past years,[5a,b,e,f,h,10] while somewhat less attention has been paid to oxide samples.[11] Oxide nanoparticles, such as silica, are important components of materials for biomedical and catalytic applications.[12] Studying their synthesis and behavior under near realistic conditions and at nanoscale in liquid-phase TEM would aid further development of their design. However, like metals, metal-oxides are sensitive to changes in chemical environment, and it is, therefore, crucial to understand which impact radiolysis species and the electron beam can have on silica nanoparticles in liquid-phase TEM.

Here, we demonstrate that the combined interaction of radiolysis species and directed electron beam irradiation led to controlled changes in the shape and size of spherical silica nanoparticles. Scanning a focused electron beam over the sample in water appeared to have the power to direct the redeposition of dissolved silica species on the side of the silica nanospheres thereby causing their elongation. Besides providing background information for future liquid-phase TEM work involving silica, this study presents a phenomenon that can potentially be employed for nanoscale manipulations.

2. Results and Discussion

2.1. Elongation of Nanoparticles

The impact of the water environment and the electron beam on the morphology of the silica nanoparticles was investigated under liquid-phase STEM conditions, and with the water being static in the liquid cell, that is in the absence of liquid flow. **Figure 1**a shows an STEM image taken at 600 000× magnification (*M*) of three silica nanoparticles spaced at least 30 nm from each other. During nearly 5 min exposure to the focused electron beam with horizontal scanning direction, the

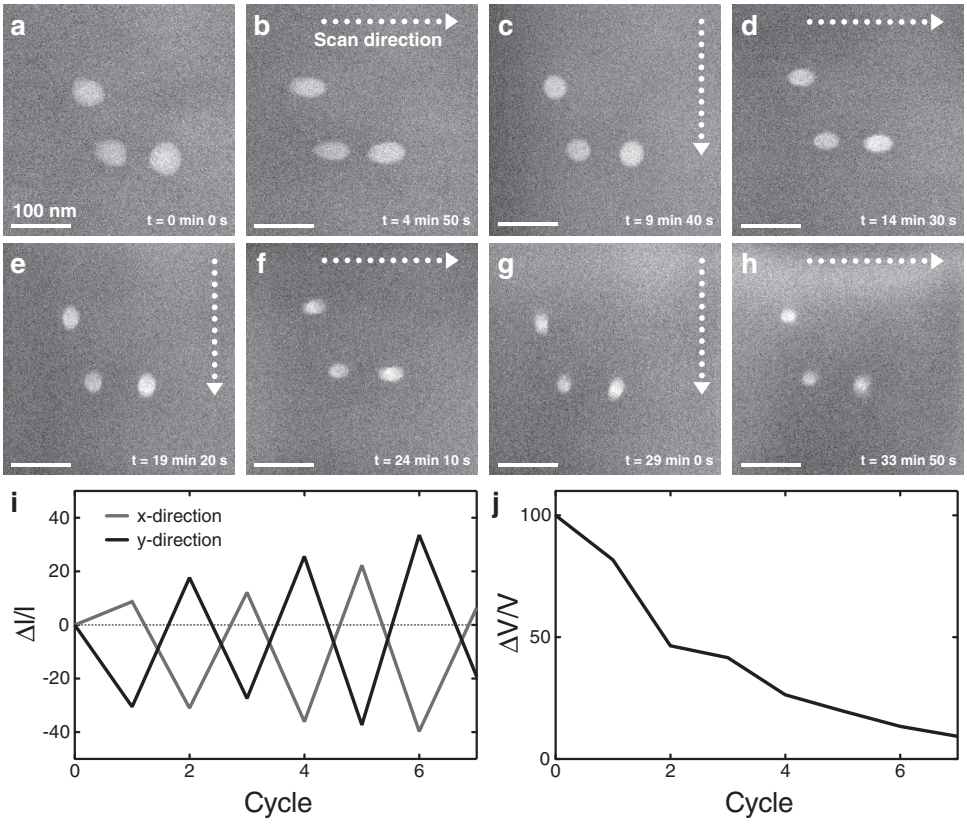

Figure 1. Liquid-phase scanning transmission electron microscopy (STEM) images of three silica nanoparticles in pure water acquired at 600 000× magnification (*M*). The electron dose rate was 3.0×10^3 e^- nm^{-2} s^{-1}. a) Image at the onset of a time-lapse series. b–h) Images recorded during the exposure to cycles of electron beam scanning with alternating horizontal and vertical directions. The scan direction is indicated on each figure with the dotted arrow along with the time that lapsed from the beginning of the experiment. Each cycle comprised of 50 STEM images; about 4 min and 50 s for each cycle, whereby only the last frame of the cycle is shown in the figures b–h. i) The average change of the sizes ($\Delta I/I$) of the nanoparticles measured in horizontal and vertical directions per cycle. The electron dose per cycle was 8.6×10^5 e^- nm^{-2}. j) The average calculated volume change ($\Delta V/I$) per cycle.

elongation of spherical silica nanoparticles in the scan direction was observed, as shown in Figure 1b. The original spherical silica nanoparticles were transformed into ellipsoidal silica nanoparticles.

To further explore the phenomenon observed in Figure 1b, the scanning direction of the electron beam was rotated by 90°, as indicated in Figure 1c, and the three silica nanoparticles were scanned for another 4 min 50 s. As can be seen in Figure 1c, the elongated silica nanoparticles from Figure 1b have returned to nearly spherical shape, however, span a smaller area in the image. In total 7 cycles with alternating horizontal/vertical scan direction were performed over nearly 34 min (Supporting Information Movie 1). In order to remove the water radiolysis species that might cause this silica reshaping and resizing, we performed additional experiments in the flow of water. However, similar effects were observed for the case of a liquid flow through the system (Figure S1, Supporting Information), pointing to either insufficient removal of the radiolysis species by water flow or the absence of their impact on the silica reshaping and resizing.

The directional changes of the nanoparticle shapes were studied from measurements of the widths of the nanoparticles in horizontal- and vertical-image directions (see Figure S2 and Table S1, Supporting Information). It appears that the width of a nanoparticle increased in a direction parallel to the scan direction, while it decreased in perpendicular direction. This directional growth reversed with the rotation of the scan direction by 90°, as shown in Figure 1i. The average increase in any scan direction amounted to 19%, while the decrease amounted to 32% on average. The nanoparticles thus became smaller from cycle to cycle. To estimate the volume, we used the measured horizontal and vertical widths, and assumed the thickness of a nanoparticle (vertical dimension perpendicular to the image plane) to be equal to the longest of the measured widths. It was indeed verified, by both examining the signal intensity and tilting the particles, that the vertical dimension did not largely reduce or increase (Figures S3 and S4, Supporting Information) during the process. The estimated volume change per cycle is shown in Figure 1j. It follows that the volume decreased to ≈10% of its original value after 7 cycles. In addition, in Figures 1g,h, light patches indicating the formation of deposit on the Si_xN_y window were observed. To investigate the chemical nature of this deposit, we performed energy dispersive X-ray analysis (EDX). It was confirmed that the deposit did not consist of silica that was dissolved from particles, but rather carbon contamination (Figure S5, Supporting Information). Furthermore, EDX showed that nanoparticles consisted of silicon oxide.

2.2. Model of Anisotropic Shape Change

Two distinct phenomena were thus observed: 1) a decrease in volume and 2) an anisotropic change of shape. Here, we propose that the apparent decrease in volume and change of shape of silica nanoparticles are a result of dissolution/redeposition of silica by the mechanism strongly influenced by the presence of both electron beam and water. The electron caused the exciting of surface silicon (in **Figure 2**a, Q^2 Si species was used as an example). The excited $Si^*(OH)_2$ was then more prone to react with water to form silicic acid—$Si(OH)_4$. Part of the formed silicic acid diffused in the liquid, hence causing the loss of silica from the nanoparticles, while another fraction dissociated to form silanolate anions—$Si(OH)_3O^-$.[13] This reaction can be particularly promoted by the change in pH, which is known to affect increase in silica dissolution. The local reduction in pH is to be expected considering that in interaction with water, electron beam leads not only to water radiolysis and formation of radicals, but also to OH^- and H^+ ions.[9a] From the data we can calculate the amount of irradiating electrons to remove an atom from the silica nanoparticle in water. The most round-appearing nanoparticle shown at the right of Figure 1a has an initial diameter of 53 nm. It was exposed to an electron dose rate of 3.0×10^3 e^- nm^{-2} s^{-1}, so that the total dose in one cycle of irradiation of 290 s amounted to 8.6×10^5 e^- nm^{-2}. A volume of 1.9×10^4 nm^3 was removed during this cycle, which translates to 4×10^5 atoms (using a density of 2.2 g cm^{-3} and a

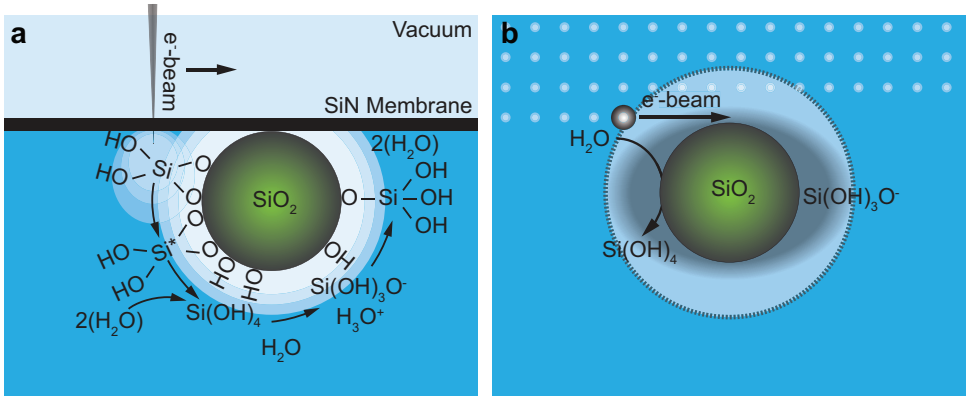

Figure 2. Schematic representation of the proposed mechanism responsible for the elongation of the silica nanoparticles. a) A focused electron beam scans over a sample in the indicated direction. The sample in water is enclosed between silicon nitride membranes containing silica nanoparticles. The electron beam reacts with the surface silicon atoms so that dissolved $Si(OH)_4$ is formed. Created silicic acid further dissociates to silanolate anion, $Si(OH)_3O^-$, of which some deposits on the nanoparticle. b) Top view of a nanoparticle. As the electron beam scans over the nanoparticle line-by-line, an increasing concentration of $Si(OH)_4$ is created in the middle region (oval shape) at which more nanoparticle surface is irradiated than at the side.

molar weight of 60 g mol^{-1}). Within the initial radiated area, the amount of electrons to remove an atom from the silica nanoparticle in water thus measured 5×10^3.

A further effect that probably took place involved the impact of the electron beam with the core of the nanoparticle via inelastic scattering, resulting in ionization and heating of the materials, and also the creation of secondary electrons. These effects tend to destabilize a material. Third, the Si_xN_y membrane probably positively charged on account of secondary electron emission,[14] which takes place upon irradiation with electron beam, attracting thus part of the dissolved silica species to be deposited at the interface between silica particle and window. Finally, direct removing atoms from the nanoparticle also occurred since the electron beam energy was above knock-on damage threshold for silicon and oxygen. But this effect was apparently not as large as the combined electron beam and water effect causing dissolution/redeposition of silica, because changes in shape and size of silica nanoparticle were not observed in vacuum for this electron dose (Figure S6, Supporting Information).

The anisotropic shape change is further explained by the combination of dissolution/redeposition process of the nanoparticle (Figure 2a) and a concentration effect (Figure 2b). Upon electron beam scanning, the electron probe first encountered the side of the nanoparticle (top in Figure 2b). As the electron probe scanned further toward the middle particle, the amount of surface silica species that were excited, dissolved, and redeposited increased, reaching a maximum in the middle of the nanoparticle. The areas at those sides of the nanoparticle scanning first and last, respectively, exhibited lower concentrations of dissolved species. This situation is reflected in Figure 2b looking from above the nanoparticle, whereby the concentration gradient of dissolved species is depicted as shaded oval shape. There is of course uncertainty about the vertical dimension of the nanoparticle but since most redeposition took place in the middle of the nanoparticle, we assumed the vertical dimension of the nanoparticle to approximately equals the long side for the calculation reflected in Figure 1j.

It should be noted that the immobilization of the nanoparticles on the supporting Si_xN_y membrane was crucial, while anisotropic concentration gradients would not build if the particles were free to move in the liquid. Yet, freely dispersed silica nanoparticles may become immobilized on the Si_xN_y membrane by the electron beam impact.[11b] The anisotropic effect was not observed for metallic nanoparticles in another study.[15]

The following other effects are listed for completeness but are unlike to have happened. It is known that an increase in temperature increases the solubility of silica in water.[16] However, it was calculated by others that a temperature increase in liquid cell is negligible,[9b] which rules out the effect of temperature on silica solubility. In theory, mass could have been transferred into the axial direction not visible in the 2D projection, thus preserving the total volume. However, this does not seem likely because ex-situ images of the nanoparticles recorded under a tilt angle did not show enlarged shapes in vertical direction (Figure S4, Supporting Information). Surface migration and electron beam sputtering may have occurred but would not have led to anisotropic shape change and, in particular, reduction in size, but would rather have distributed material homogenously over the surface. Plastic deformation of the nanoparticle upon irradiation was published for ion-beam irradiation of silica nanoparticles in vacuum.[17] Those authors found an expansion of the nanoparticle in a direction perpendicular to the ion beam caused by local heating of the particle. This effect did not likely happen in our experiment because in the plane perpendicular to the beam, the nanoparticles showed both, expansion and compression. Moreover, the nanoparticles were surrounded by liquid with excellent heat conducting properties so that significant temperature changes did not likely occur. The observed process is different from experiments in vacuum (Figure S6, Supporting Information) where some structural rearrangement takes places at very high electron doses but growth in one direction and shrinkage in the perpendicular direction is not observed.[12d]

2.3. Creating Holes at Higher Electron Doses

Upon increasing the magnification, and consequently the total electron dose rate to which the nanoparticles were exposed, another interesting phenomenon was observed as well. In **Figure 3**, three separate measurements of single silica nanoparticles performed at increasing magnifications are shown. The first two measurements were performed with water being static in the cell, while the third measurement at M = 1 500 000× was performed under the flow of phosphate buffered saline (PBS). During scanning with the electron beam in horizontal direction, dark oval shapes appeared in all three silica nanoparticles oriented in the same direction as the nanoparticle elongation. The dark patches indicate a loss of material from the centers of the nanoparticles because the dark field contrast of STEM results in a lower signal level at locations with lower mass for a sample of the same density (Figure S7, Supporting Information).

The level of structural degradation of the silica nanoparticles became more pronounced with increasing magnification, that is, electron dose rate (Figure 3a–c, second from the left column of images). The holes vanished after 4 min 50 s of imaging at the highest doses, while the silica nanoparticles became smaller at all doses (Figure 3b,c, second from the right column of images). At M = 1 500 000× the nanoparticle was only faintly visible after 4 min 50 s, indicating a significant loss of material. Low magnification images recorded after 4 min 50 s scanning (Figure 3a–c, rightmost images), depict lighter patches corresponding to deposits in the areas exposed to the scanning electron beam. This change in contrast was again attributed to deposition of carbon at the vacuum side of the Si_xN_y window (Figure S8, Supporting Information).

Using a salt solution instead of pure water should increase the electrical conductance of the liquid, and possibly reduce the impact of free electrons and charging. However, STEM of silica nanoparticles in PBS at M = 1 500 000× showed larger shape changes than for pure water at M = 1 200 000× (Figure 3b,c). Thus, imaging in PBS did not lead to a large

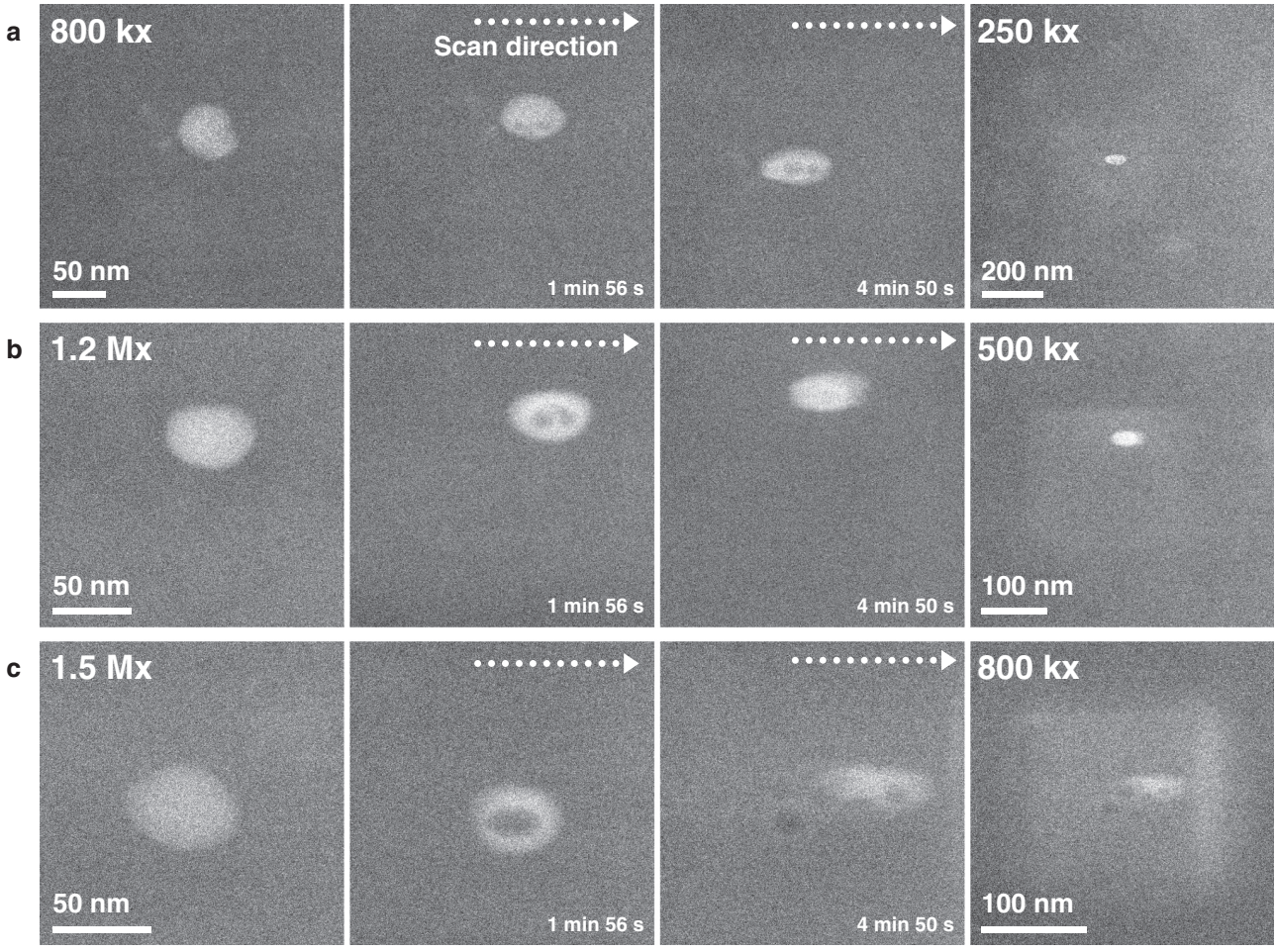

Figure 3. Liquid-phase STEM time-lapse experiment of individual silica nanoparticles at increasing magnification. a) Row of four images of nanoparticles in pure water, $M = 800\,000\times$. b) Row of images in pure water recorded at $M = 1\,200\,000\times$. c) Images of nanoparticles in flow of PBS solution, $M = 1\,500\,000\times$. The leftmost images of columns a–c show silica nanoparticles before the prolonged exposure to the scanning electron beam. After 1 min 56 s of horizontal electron beam scanning (second image column from the left), dark areas appeared within the nanoparticles indicating a loss of material from their centers. The higher the magnification was, the larger the loss of material. The nanoparticles increasingly elongated and reduced their size upon prolonged electron beam scanning, and the effect was the strongest for the highest magnification. Lower magnification images (rightmost column) show a deposition of material in the exposed area.

reduction of the electron beam effect comparing to the situation in pure water. Switching the water flow on, the same phenomenon of silica nanoparticles elongating and shrinking was observed, along with the formation of hollow silica nanoparticles upon using higher magnifications (Figure 3c).

2.4. Elongation of Nanoparticles in Aggregates

The behavior of an aggregate of silica nanoparticles under STEM conditions was also investigated. The liquid consisted of either pure water or PBS and was flown through the liquid cell. Comparing **Figure 4**a left with second from left it can be seen that the silica nanoparticles elongated already after 4 min 50 s of scanning in horizontal direction. The volume reduction was particularly pronounced after the second scan as the nanoparticles returned to a nearly spherical shape (Figure 4a, middle panel). In addition to the shape and size changes of the individual silica nanoparticles, it was observed that the entire aggregate elongated upon horizontal electron beam scanning. After changing the scanning direction to vertical, and exposing the agglomerate to another 4 min 50 s of scanning, the aggregate returned to its original spherical shape but of a reduced size.

Possibly, the interparticle porosity reduced compared to its original structure. It was also found that silica nanoparticles fused, turning the porous silica aggregate (i.e., loosely bound silica particles) into a solid-appearing agglomerate (i.e., particles bound by fusion or sintering) of low porosity as was also observed in a previous study.[11b] After the fifth cycle of scanning had finished (in total about 24 min under electron beam), the size of the silica aggregate was reduced to about half its original size (Figure 4a, rightmost). The same effect of the electron beam on a silica aggregate was observed when water was used instead of PBS (Figure 4b). This experiment revealed an even more pronounced elongation of the individual silica nanoparticles and the aggregate as a whole, ascribed to the higher used magnification and

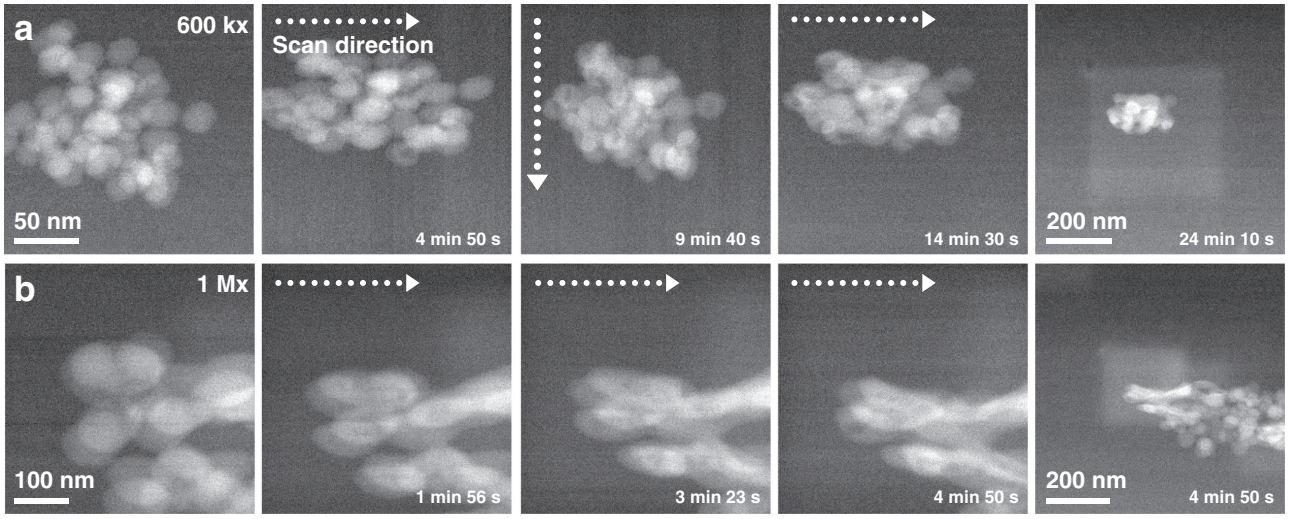

Figure 4. Liquid-phase STEM of aggregates of silica spheres in a flow of liquid. a) PBS solution and in a flow of b) pure water using STEM. a) Silica aggregate in a flow of PBS imaged at M = 600 000× over a period of about 24 min, with in total of 5 cycles of alternating scan direction (three shown here). b) Silica aggregate in pure water was imaged at M = 1 000 000× over a period of 4 min 50 s with the electron beam scanning in the indicated direction. The rightmost figures show low magnification images completing the experiment.

electron dose. Since drastic elongation and fusion of silica nanoparticles already took place after 1 min 56 s, scanning was only performed in one direction. The directional effect of the scanning electron beam on the shape change of the silica aggregate is best observed at lower magnification (Figure 4b, rightmost). It can be seen that the part of the aggregate that was exposed to the scanning electron beam was completely deformed, while the remaining part of the aggregate still contained spherical silica nanoparticles. Additionally, lighter areas in the scanned region corresponding to deposits of carbon were observed.

2.5. TEM Experiments

Our results indicate that the focused electron beam of STEM has the capability to reshape silica nanoparticles in aqueous environment. We thus expected that no directional shape change should occur in case of TEM, where the electron beam illuminates the entire field of view instead of being focused, and is not raster-scanned across the sample as in STEM. Indeed, when silica nanoparticles were imaged using TEM, no elongation or other directional shape changes were seen (**Figure 5**). Figure 5a shows an aggregate of silica nanoparticles examined under water flow conditions in liquid-phase TEM over a 10 min period. The shrinkage of the silica aggregates was evident, and accompanied by the fusion of several silica nanoparticles. That silica nanoparticles can completely dissolve under these conditions was confirmed by imaging isolated silica nanoparticles at a higher magnification (Figure 5b). The silica nanoparticle shapes almost completely disappeared after ≈10 min. It is assumed that the nanoparticles dissolved but it cannot be entirely ruled out that a carbon contamination layer was formed reducing the contrast. Nevertheless, in both cases, no elongation of the silica nanoparticles was observed for TEM.

3. Conclusions and Outlook

In this work, we have demonstrated that the shape and size of silica nanoparticles in a water environment can be manipulated anisotropically by the impact of a focused electron beam. Four distinct effects were observed. First, silica nanoparticles dissolved as was evident from a gradual reduction of their size. Second, dissolved silica species were redeposited on the edges of the silica nanoparticles leading to an elongation of the nanoparticles in the scan direction. Third, more material was removed from the center of the nanoparticles than from their edges at higher electron dose rates, so that doughnut-shaped objects were generated. For the case of silica nanoparticles assembled in aggregates, finally, we observed both the fusing of neighboring nanoparticles and the elongation of the entire section of the aggregate exposed to the electron beam. Notably, the directional redeposition did not take place under liquid-phase TEM conditions. These observations provide new information about the behavior of silica nanoparticles under liquid-phase STEM and TEM conditions. These effects should be considered when designing liquid-phase electron microscopy experiments aiming for observing processes happening at the surface of silica nanoparticles. Low dose conditions or a careful selection of the liquid to prevent dissolution of silica would be required to preserve the original structure of the silica nanoparticles, as was shown possible for gold nanoparticles.[14] As is apparent from the elongation of irradiated nanoparticles in aggregates, it is also possible to modify arrays of silica nanoparticles in parallel. These processes may find future application to the controlled manipulation of the size and the shape of

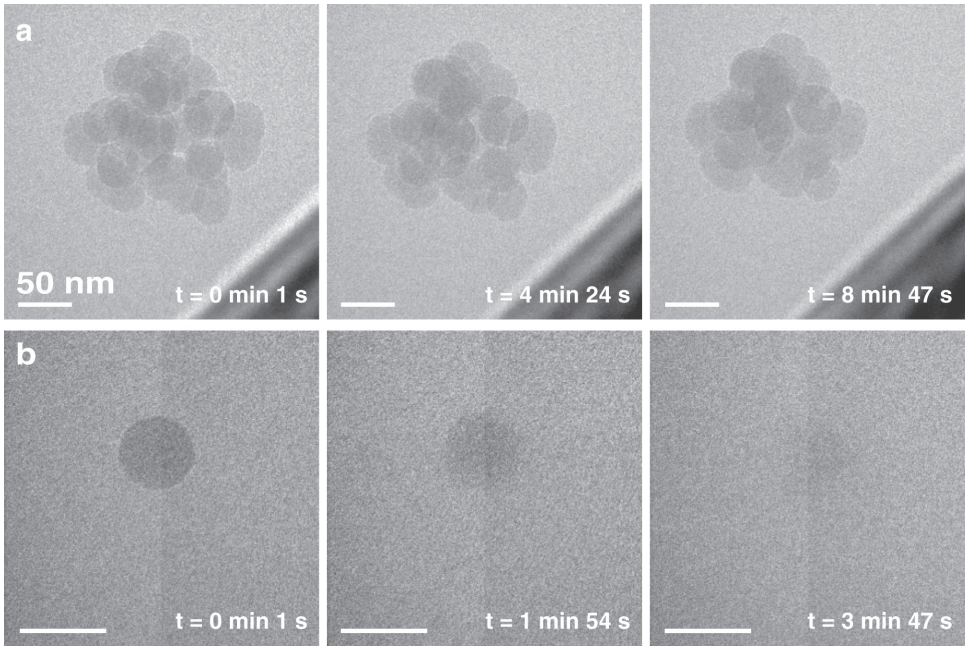

Figure 5. Liquid-phase TEM of silica nanoparticles in a flow of pure water. a) An aggregate imaged at M = 250 000×. b) An isolated nanoparticle at M = 400 000×. Each 5 s a new image was acquired, leading to a total of 100 frames in 9 min 48 s. Silica dissolved with elapsing time. Scale bars are 50 nm.

nanomaterials in liquid, whereby materials are created with different properties in different orientations.

4. Experimental Section

Sample Preparation: Spherical monodispersed nanoparticles of silica with an average diameter of 50 ± 5 nm were prepared via a procedure adopted from Stoeber et al.[18] A mixture containing of ethanol (230 mL) and of ammonia (11.25 mL, Merck, 25%) was stirred, and heated to 35 °C. Tetraethyl orthosilicate (7.3 g, TEOS, Aldrich, 98%) was then added, and the solution left to stir for 15 h at 35 °C. The solution was neutralized with nitric acid (Merck, 65%) and liquid removed using a rotary evaporator. Solid (silica) was dried overnight at 120 °C, and calcined in air for 2 h at 200 °C, followed by 1 h at 400 °C and finally 3 h at 600 °C. To break the aggregated nanoparticles and thus to expose as much as possible individual silica spheres, the sample was dispersed in ethanol and sonicated for about 15 min.

Loading of the Liquid Specimen TEM Holder: A droplet (0.2 µL) of silica–ethanol suspension was placed on top of an Si microchip (Protochips Inc., NC, USA) supporting an Si_xN_y window of 50 nm thickness and dimensions of 20 × 200 µm^2. The microchip was plasma cleaned prior to loading to render the surface hydrophilic, and silica spheres were dispersed on the surface of the microchip. A dried microchip with silica was then positioned in the tip of a dedicated liquid-phase TEM holder (Protochips Inc., NC, USA), and a droplet (0.5 µL) of either pure water or diluted (1:100) phosphate buffer saline solution (Roti-Stock 10x, PBS) was placed on top. The liquid cell was then closed by placing the second microchip on top, with its membrane side facing downward. In this configuration, the microchip with silica nanoparticles was the top one once the holder was inserted in the electron microscope, such that the highest possible spatial resolution was obtained in the STEM mode for the downward traveling electron beam.[2,19]

Electron Microscopy: Imaging was performed using an ARM200F (JEOL, Japan) microscope in either STEM or TEM mode at 200 keV electron beam energy. The following settings were used for STEM experiments: a probe current of 80 pA (adjusted on the microscope by selecting spot size 6C, and 40 µm condenser lens aperture), and 8 cm camera length. STEM images of 512 × 512 pixels were collected with 20 µs pixel-dwell time. The image frame time in a time-lapse STEM image series was 5.2 s. The electron dose for an image recorded at a typical magnification of 600 000× and a pixel size of 0.8 nm thus amounted to 1.6×10^4 e$^-$ nm^{-2} (assuming that the electron dose was homogeneously distributed over a pixel area as a result of electron scattering by the silicon nitride membrane, nanoparticles, and the liquid). The electron dose rate in a time-lapse STEM image series was thus 3.0×10^3 e$^-$ nm^{-2} s^{-1}. During the experiments, water or PBS solutions were either kept static or flown at 4 µL min^{-1} through the cell. The TEM experiments were performed using 200 keV acceleration voltage, spot size 1, condenser lens aperture 1, and objective aperture 2. In case of TEM experiments, the sample was dispersed on the other microchip so that it was at the bottom one once the holder is inserted in the microscope, thus providing the best resolution for TEM.[2,20]

TEM images had a size of 1024 × 1024 pixels and the image acquisition time was 1 s.

Supporting Information

Supporting Information is available from the Wiley Online Library or from the author.

Acknowledgements

R. van den Berg and T. Parmentier are thanked for providing silica samples. J.Z. and K.J. acknowledge funding from the NRSCC and European Research Council, an EU FP7 ERC Advanced Grant no. 338846. N.J. thanks Protochips Inc., NC, USA, for providing the liquid-phase TEM system, and E. Arzt for his support through INM.

[1] a) J. Zecevic, K. P. de Jong, P. E. de Jongh, *Curr. Opin. Solid State Mater. Sci.* **2013**, *17*, 115; b) A. K. Datye, *J. Catal.* **2003**, *216*, 144; c) C. Kiely, *Nat. Mater.* **2010**, *9*, 296.

[2] a) N. de Jonge, F. M. Ross, *Nat. Nanotechnol.* **2011**, *6*, 695; b) J. M. Grogan, N. M. Schneider, F. M. Ross, H. H. Bau, *J. Indian Institute Sci.* **2012**, *92*, 295; c) C. M. Wang, H. G. Liao, F. M. Ross, *MRS Bull.* **2015**, *40*, 46; d) X. Y. Yu, B. W. Liu, L. Yang, *Microfluid. Nanofluid.* **2013**, *15*, 725; e) D. F. Parsons, *Science* **1974**, *186*, 407.

[3] a) M. J. Williamson, R. M. Tromp, P. M. Vereecken, R. Hull, F. M. Ross, *Nat. Mater.* **2003**, *2*, 532; b) K. L. Liu, C. C. Wu, Y. J. Huang, H. L. Peng, H. Y. Chang, P. Chang, L. Hsu, T. R. Yew, *Lab Chip* **2008**, *8*, 1915; c) H. Zheng, S. A. Claridge, A. M. Minor, A. P. Alivisatos, U. Dahmen, *Nano Lett.* **2009**, *9*, 2460; d) M. J. Dukes, B. W. Jacobs, D. G. Morgan, H. Hegde, D. F. Kelly, *Chem. Commun.* **2013**, *49*, 3007; e) E. Jensen, C. Kobler, P. S. Jensen, K. Molhave, *Ultramicroscopy* **2013**, *129*, 63; f) T. J. Woehl, K. L. Jungjohann, J. E. Evans, I. Arslan, W. D. Ristenpart, N. D. Browning, *Ultramicroscopy* **2013**, *127*, 53.

[4] J. Y. Huang, L. Zhong, C. M. Wang, J. P. Sullivan, W. Xu, L. Q. Zhang, S. X. Mao, N. S. Hudak, X. H. Liu, A. Subramanian, H. Fan, L. Qi, A. Kushima, J. Li, *Science* **2010**, *330*, 1515.

[5] a) H. Zheng, R. K. Smith, Y. W. Jun, C. Kisielowski, U. Dahmen, A. P. Alivisatos, *Science* **2009**, *324*, 1309; b) J. E. Evans, K. L. Jungjohann, N. D. Browning, I. Arslan, *Nano Lett.* **2011**, *11*, 2809; c) D. Li, M. H. Nielsen, J. R. Lee, C. Frandsen, J. F. Banfield, J. J. De Yoreo, *Science* **2012**, *336*, 1014; d) H. L. Xin, H. Zheng, *Nano Lett.* **2012**, *12*, 1470; e) T. J. Woehl, J. E. Evans, L. Arslan, W. D. Ristenpart, N. D. Browning, *ACS Nano* **2012**, *6*, 8599; f) K. L. Jungjohann, S. Bliznakov, P. W. Sutter, E. A. Stach, E. A. Sutter, *Nano Lett.* **2013**, *13*, 2964; g) P. J. Smeets, K. R. Cho, R. G. Kempen, N. A. Sommerdijk, J. J. De Yoreo, *Nat. Mater.* **2015**, *14*, 394; h) T. Kraus, N. de Jonge, *Langmuir* **2013**, *29*, 8427.

[6] a) E. A. Ring, N. de Jonge, *Micron* **2012**, *43*, 1078; b) X. Chen, J. Wen, *Nanoscale Res. Lett.* **2012**, *7*, 598; c) E. R. White, M. Mecklenburg, B. Shevitski, S. B. Singer, B. C. Regan, *Langmuir* **2012**, *28*, 3695.

[7] a) A. Radisic, P. M. Vereecken, J. B. Hannon, P. C. Searson, F. M. Ross, *Nano Lett.* **2006**, *6*, 238; b) M. Gu, L. R. Parent, B. L. Mehdi, R. R. Unocic, M. T. McDowell, R. L. Sacci, W. Xu, J. G. Connell, P. H. Xu, P. Abellan, X. L. Chen, Y. H. Zhang, D. E. Perea, J. E. Evans, L. J. Lauhon, J. G. Zhang, J. Liu, N. D. Browning, Y. Cui, I. Arslan, C. M. Wang, *Nano Lett.* **2013**, *13*, 6106; c) R. L. Sacci, N. J. Dudney, K. L. More, L. R. Parent, I. Arslan, N. D. Browning, R. R. Unocic, *Chem. Commun.* **2014**, *50*, 2104; d) D. Alloyeau, W. Dachraoui, Y. Javed, H. Belkahla, G. Wang, H. Lecoq, S. Ammar, O. Ersen, A. Wisnet, F. Gazeau, C. Ricolleau, *Nano Lett.* **2015**, *15*, 2574.

[8] a) D. B. Peckys, N. de Jonge, *Microsc. Microanal.* **2014**, *20*, 346; b) H. Nishiyama, M. Suga, T. Ogura, Y. Maruyama, M. Koizumi, K. Mio, S. Kitamura, C. Sato, *J. Struct. Biol.* **2010**, *169*, 438; c) B. L. Gilmore, S. P. Showalter, M. J. Dukes, J. R. Tanner, A. C. Demmert, S. M. McDonald, D. F. Kelly, *Lab Chip* **2013**, *13*, 216.

[9] a) N. M. Schneider, M. M. Norton, B. J. Mendel, J. M. Grogan, F. M. Ross, H. H. Bau, *J. Phys. Chem. C* **2014**, *118*, 22373; b) J. M. Grogan, N. M. Schneider, F. M. Ross, H. H. Bau, *Nano Lett.* **2014**, *14*, 359.

[10] J. M. Yuk, J. Park, P. Ercius, K. Kim, D. J. Hellebusch, M. F. Crommie, J. Y. Lee, A. Zettl, A. P. Alivisatos, *Science* **2012**, *336*, 61.

[11] a) K. L. Jungjohann, J. E. Evans, J. A. Aguiar, I. Arslan, N. D. Browning, *Microsc. Microanal.* **2012**, *18*, 621; b) M. W. van de Put, C. C. Carcouet, P. H. Bomans, H. Friedrich, N. de Jonge, N. A. Sommerdijk, *Small* **2015**, *11*, 585; c) D. S. Li, M. H. Nielsen, J. J. De Yoreo, *Methods Enzymol.* **2013**, *532*, 147.

[12] a) M. Liong, J. Lu, M. Kovochich, T. Xia, S. G. Ruehm, A. E. Nel, F. Tamanoi, J. I. Zink, *ACS Nano* **2008**, *2*, 889; b) S. H. Joo, J. Y. Park, C. K. Tsung, Y. Yamada, P. D. Yang, G. A. Somorjai, *Nat. Mater.* **2009**, *8*, 126; c) G. Prieto, J. Zecevic, H. Friedrich, K. P. de Jong, P. E. de Jongh, *Nat. Mater.* **2013**, *12*, 34; d) R. van den Berg, T. E. Parmentier, C. F. Elkjaer, C. J. Gommes, J. Sehested, S. Helveg, P. E. de Jongh, K. P. de Jong, *ACS Catal.* **2015**, *5*, 4439.

[13] G. B. Alexander, W. M. Heston, R. K. Iler, *J. Phys. Chem.* **1954**, *58*, 453.

[14] A. Verch, M. Pfaff, N. De Jonge, *Langmuir* **2015**, *31*, 6956.

[15] J. Hermannsdoerfer, N. de Jonge, A. Verch, *Chem. Commun.* **2015**, *51*, 16393.

[16] S. H. A. Chan, *Geothermics* **1989**, *18*, 49.

[17] T. van Dillen, A. Polman, C. M. van Kats, A. van Blaaderen, *Appl. Phys. Lett.* **2003**, *83*, 4315.

[18] W. Stoeber, A. Fink, E. Bohn, *J. Colloid Interface Sci.* **1968**, *26*, 62.

[19] a) N. de Jonge, N. Poirier-Demers, H. Demers, D. B. Peckys, D. Drouin, *Ultramicroscopy* **2010**, *110*, 1114; b) T. Schuh, N. de Jonge, *C. R. Phys.* **2014**, *15*, 214.

[20] K. L. Klein, I. M. Anderson, N. de Jonge, *J. Microsc.* **2011**, *242*, 117.

Received: July 25, 2016
Revised: August 25, 2016
Published online: October 13, 2016

